Desalination and Water Treatment
www.deswater.com

doi: 10.5004/dwt.2023.29810

308 (2023) 102–109
October

Study on the adsorption of phosphate over biochar-based adsorbents from peanut shell and orange peel in water

Yue Zhao[a], Xue He[b], Kezhen Qi[b,*], Amir Zada[c,*], Jing Pan[a,*]

[a]*College of Life Science, Shenyang Normal University, Shenyang 110034, China, emails: crystalpan@synu.edu.cn (J. Pan), ZhaoY_0234@163.com (Y. Zhao)*
[b]*College of Pharmacy, Dali University, Dali 671000, China, emails: qkzh2003@aliyun.com (K. Qi), hexue2023du@163.com (X. He)*
[c]*Department of Chemistry, Abdul Wali Khan University, Mardan, Khyber Pakhtunkhwa 23200, Pakistan, email: amistry009@yahoo.com (A. Zada)*

Received 15 April 2023; Accepted 26 July 2023

ABSTRACT

The presence of complex functional groups and a well-developed pore structure make biochars highly effective in the removal of hazardous substances from water. In this work, peanut shell and orange peel biochars were produced by slow pyrolysis at different temperatures (300°C, 400°C, 500°C) for 6 h. The prepared biochars were used to treat phosphate in water to explore the effect of contact time and initial concentration of phosphate on adsorption performance. The kinetic models were fitted to study the adsorption mechanisms. The results showed that the highest yields of peanut shell (86.7%) and orange peel biochars (81.2%) were achieved at 400°C and 300°C, respectively. 5.0 g of peanut shell biochars removed about 5.94 mg/g phosphate in 26 h and the removal rate was 83.2%, while the same amount of orange peel biochars removed about 5.79 mg/g phosphate in 26 h and the removal rate was 81.1%. The adsorption processes of phosphate by peanut shell and orange peel biochars fitted with the secondary kinetic models, which were dominated by chemical adsorption.

Keywords: Water eutrophication; Adsorption; Biochar; Phosphate; Dynamic model

1. Introduction

The advent of industrialization has caused serious damage to the environment. Many organic and inorganic compounds such as dyes, halogenated aromatic compounds, acids, bases, heavy metals etc have been loaded to the external environment from different industries [1,2]. The presence of these compounds has caused serious damage to both aquatic and terrestrial plants and animals. Particularly, due to their high thermal stability and resistant to biodegradation, these compounds are slowly accumulated in water bodies beyond their limited concentration [3–6]. Similarly, the presence of inorganic compounds of phosphorous, sulphur, alkali, and alkaline earth metals are also present in different segments of the environment with enormous hazardous application [7–11]. In order to keep our environment clean and safe for future generations, these compounds must be eradicated preferentially to avoid their hazardous application.

Phosphorus is not only a vital component of human dental and skeletal structures, but also a crucial element that impacts the growth and development of plants [12]. However, high concentration of phosphorus which is usually present in the form of phosphate in water environment has many side effects including reduction in plant growth and oxygen solubility [13]. This reduction in oxygen solubility causes death of aquatic organisms and seriously damages the quality of groundwater. The rate of eutrophication is increased many folds due to the excessive use of chemical fertilizers in agricultural production, development of

* Corresponding author.

aquaculture, and use of phosphorus containing detergents to produce urban domestic sewage [14]. Therefore, reduction in the concentration of phosphate in water bodies and deceleration of the eutrophication rate are very important environmental problem to be solved urgently [15].

In recent years, biochar has become one of the most attractive materials in water purification due to its low cost and excellent adsorption capability for many pollutants [16–18]. Biochar is generally produced by properly heating plant residues under oxygen-free or oxygen-limited conditions in the temperature range of 300°C–1,000°C [19,20]. Its large specific surface area due to porous structure and presence of different functionalities play important role in the eradication of hazardous adsorbents [21–26]. Gong et al. [27] loaded biochar with bismuth particles to form microporous structure and improve the specific surface area. The resultant adsorbent removed significant amount of phosphate as governed by the spontaneous endothermic adsorption. He et al. [28] using calcium modified biochar found that the adsorption capability of the adsorbent was the highest for phosphate removal when the mass ratio of calcium hydroxide to flour was 2:1, and the whole adsorption process was fully fitted with Langmuir and pseudo-secondary model. Sizmur et al. [29] used magnesium chloride as a modifier to prepare biochar from different raw materials and found that the adsorption effect of banana straw biochar-based adsorbent for phosphate was the highest with the adsorption amount of 31.15 mg/g. The adsorption mechanism was mainly surface electrostatic attraction, Mg^{2+} precipitation and complexation with surface hydroxyl functional groups.

To eradicate phosphate from wastewater through adsorption, biochar-based adsorbents were prepared from peanut shell and orange peel in this research work. The materials were heated at elevated temperature (300°C, 400°C and 500°C) to improve the surface morphology and porous structure of the resultant adsorbents. The surface morphology and structure of the prepared biochar-based adsorbents were investigated through scanning electron microscopy (SEM) and Brunauer–Emmett–Teller (BET) techniques. The adsorptive performance of the adsorbents was studied by exploring the effect of reaction time and phosphate concentration on the adsorption efficiency. The obtained data was fitted with the second-order kinetic model to clarify the whole adsorption process and mechanism. We hope that this work will provide a reference for the application of biochar-based materials in wastewater treatment.

2. Materials and methods

2.1. Raw materials and reagents

White sand peanut shells and ugly orange peels were chosen as raw materials for the production of biochars. Analytical grade ascorbic acid, ammonium molybdate tetrahydrate, potassium dihydrogen phosphate, potassium tartrate and potassium persulfate were respectively purchased from Tianjin Institute of Chemical Reagents (China), Shenyang Chemical Reagent Factory (China), Tianjin Kemio Chemical Reagent Co., Ltd., (China), Liaoning Yongqiang Pharmaceutical Instrument Glass Co., Ltd., (China), and Tianjin Ruijinte Chemical Co., Ltd., (China).

2.2. Preparation of biochars

The peanut shells and orange peels were initially subjected to a thorough deionized water wash followed by gentle oven drying. The dried materials were placed in an electric blast drying oven and subjected to a drying process at 105°C for 48 h. Subsequently, they were pulverized into powder using a pulverizer. After being sieved through a 100-mesh sieve, the powdered materials were transferred to a crucible and subjected to carbonization in a muffle furnace at different temperatures (300°C, 400°C and 500°C) for a duration of 6 h. After being cooled to room temperature, the powder was thoroughly rinsed with ultra-pure water until it reached a neutral pH. It was then dried until reaching a constant weight and stored in a sealed bag within a desiccator.

2.3. Characterization of the biochars

The morphologies of the biochars prepared were examined using a scanning electron microscope (SEM, FEI Quanta FEG 450, US) at scan rates of 1, 5 and 10 μm. The specific surface area and pore size of the biochars were determined using the BET multi-point method and Barrett–Joyner–Halenda theory, respectively. MicroActive ASAP 2460 was employed to analyze the BET surface area and pore structure.

2.4. Yield calculation

The biochar yields were determined by utilizing the masses of the materials pre- and post-carbonization, as outlined in Eq. (1):

$$\eta(\%) = \frac{M_1}{M_2} \times 100 \tag{1}$$

where η represents the percentage yield, while M_1 and M_2 denote the masses of the powdered materials before and after carbonization respectively, measured in grams [30].

The removal rate of phosphate was calculated by Eq. (2):

$$\text{Removal rate}(\%) = \frac{(C_o - C_e)}{C_o} \times 100\% \tag{2}$$

where C_o and C_e is the initial and final concentration of phosphate, mg/L.

The adsorption capacity of biochar was calculated by Eq. (3):

$$Q_e = \frac{(C_o - C_e)V}{M} \tag{3}$$

where C_o is the initial concentration and C_e is the final equilibrium concentration of simulated phosphate solution, mg/L. V is the volume of phosphate solution, L. M is the mass of the biochars, g.

2.5. Configuration and measurement of phosphorous in wastewater

The compound potassium dihydrogen phosphate was utilized to prepare an aqueous solution with a phosphate

concentration of 0.5 mg/L. Total phosphate was quantified using ammonium molybdate-based spectrophotometry. The sample solution was digested for 30 min, followed by the addition of ascorbic acid and then molybdate solution. After standing for 15 min, the concentration of phosphate was measured using a multi-parameter water quality analyzer. Ultra-pure water with a resistance of 18 MΩ was used in this experiment.

2.6. Design of the adsorption experiment

2.6.1. Effect of contact time

A controlled variable method was employed to investigate the factors influencing the rate of removal and adsorption capacity of biochars. A quantity of 5.0 g of biochars were taken and introduced into a 100 mL aqueous solution with a phosphate concentration of 0.5 mg/L. The mixture was placed in a temperature-controlled oscillation box at ambient conditions and agitated at a speed of 180 rpm in a water bath. At regular time intervals (24, 26, 28, and 30 h), 1 mL of the solution was extracted to determine the concentration of total phosphate. Each experiment was conducted in triplicate to investigate the impact of contact time on the adsorption capacity of the biochars and phosphate removal rate.

2.6.2. Effect of concentration

A total of 5.0 g of biochars was added to a 100 mL aqueous solution containing different phosphate concentrations (0.3, 0.5, 1.0, and 1.3 mg/L). The mixture was placed in a constant temperature oscillation box at room temperature and agitated at a speed of 180 rpm in a water bath. After 28 h, a sample of 1 mL solution was collected to determine the concentration of total phosphate. Each experiment process was conducted three times to investigate the impact of phosphate concentration on the adsorption capacity of the adsorbents.

3. Results and discussion

3.1. Biocarbon yield

The biochar yields from peanut shells and orange peels are presented in Fig. 1, which were influenced by various experimental conditions such as temperature, contact time and feedstock type. As the raw material is subjected to high temperatures for an extended period, complete carbonization occurs, resulting in the separation of functional groups and a simultaneous increase in carbon content while reducing hydrogen and oxygen contents [31]. From the perspective of raw material types, the overall biochar yields of peanut shells exceeded that of orange peels, with an average yield exceeding 80%. The maximum yields for peanut shell biochars and orange peel biochars were achieved at 86.7% when pyrolyzed at 400°C for 6 h and at 81.2% when pyrolyzed at 300°C for 6 h, respectively. The reason for this is that peanut shells contain more than 60% crude fiber, which can be easily carbonized and thus lead to a higher ash content. In contrast, orange peels primarily consist of volatile oil and flavonoids, which are more difficult to carbonize under the given conditions [32].

3.2. Influence of the contact time on adsorption process

The change in phosphate removal rate and adsorption capacity of biochars derived from peanut shells and orange peels with contact time is illustrated in Fig. 2. The trend in phosphate removal and adsorption capacity of biochars remained relatively consistent as the contact time increased, despite variations in carbonization temperatures, contact times and raw materials. The adsorption of phosphate onto biochars derived from peanut shells and orange peels initially increased, reaching equilibrium after 26 h. At this time, the peanut shell biochars carbonized for 6 h at 400°C exhibited a phosphate removal rate of 81.33% and a maximum adsorption amount of 5.91×10^{-3} mg/g, while the orange peel biochars carbonized for 6 h at 300°C showed a phosphate removal rate of 74.84% and a maximum adsorption amount of 5.27×10^{-3} mg/g. The biochars produced from orange peels carbonized at 300°C and the biochar produced from peanut shell carbonized at 400°C for 6 h exhibited superior adsorption capabilities. The adsorption capacity of peanut shell biochars for phosphate is superior to that of orange peel biochars. The reason is that peanut shells contained more calcium (0.25%~0.27%) and iron (0.12%~0.18%) polyvalent metal components than orange peels (0.055%~0.082% calcium, 0.03%~0.08% iron) in this study. The poor content of multivalent metal elements in common used biomasses impede the efficiencies of their biochars [33–36]. Thus, biochars from biomasses rich in these elements are more feasible in phosphorus removal.

3.3. Effect of initial concentration of phosphate

The effect of initial phosphate concentration on the phosphate removal rate and adsorption capacity of biochars derived from peanut shells and orange peels is illustrated in Fig. 3. The impact of the initial phosphate concentration on the adsorption ability of both biochars is clearly evident. The trend in phosphate removal exhibited a general resemblance as the initial phosphate concentration

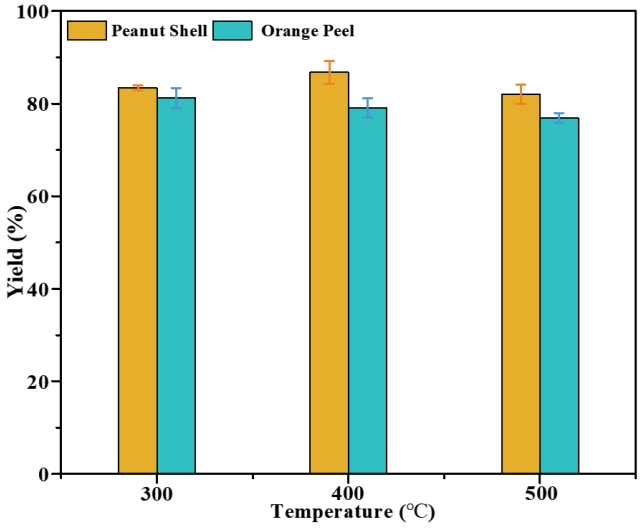

Fig. 1. Yields of biochars from peanut shells and orange peels at different temperatures.

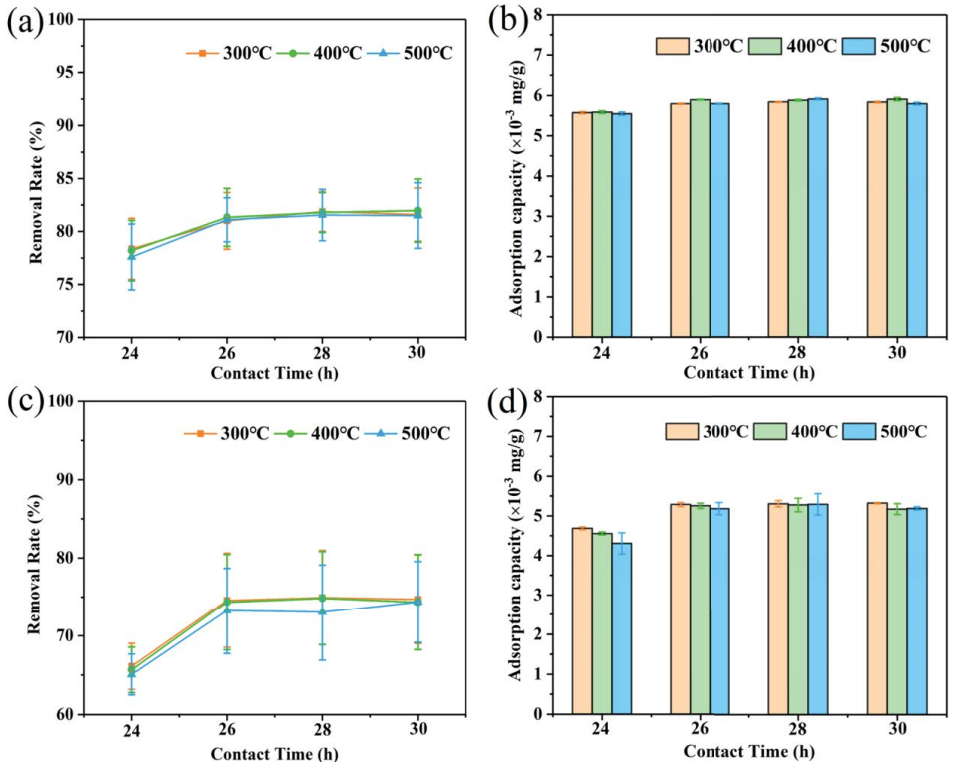

Fig. 2. Removal rate and adsorption capacity of biochars produced from peanut shells (a,b) and orange peels (c,d) at different contact times.

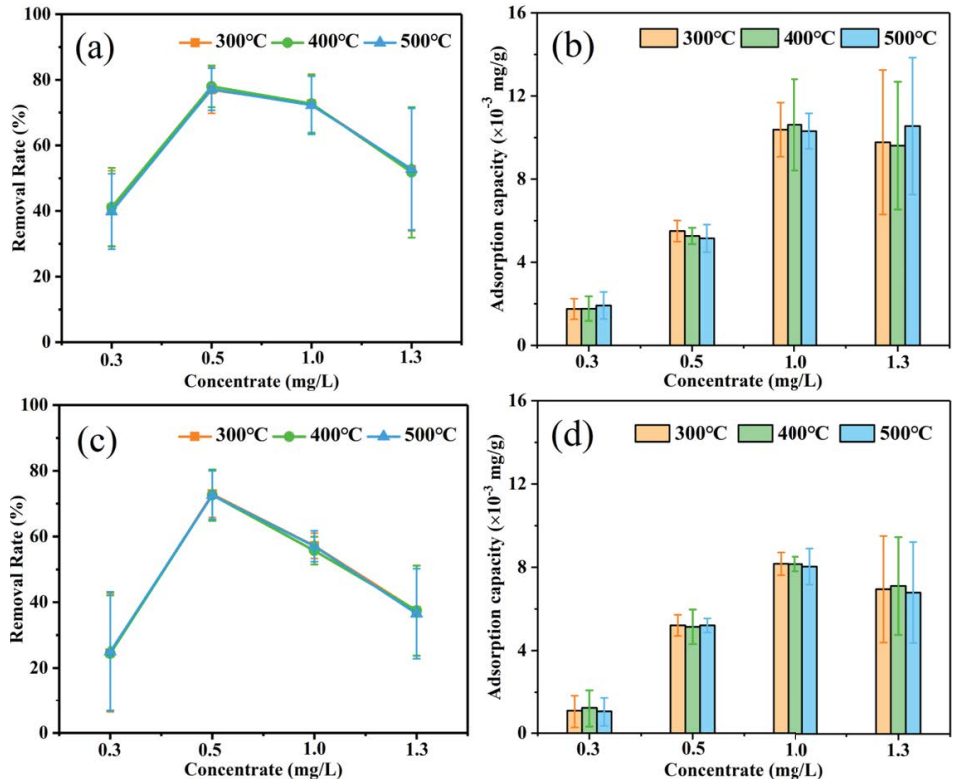

Fig. 3. Removal rate and adsorption capacity of biochars produced from peanut shells and orange peels at different initial concentrations of phosphate.

increased. Initially, there was a significant increase in the adsorption of phosphate by peanut shell biochars, followed by reaching a plateau and ultimately declining. When the initial phosphate concentration was 0.5 mg/L, the maximum removal rate reached 81.74%. As the initial phosphate concentration increased to 1.0 mg/L, a maximum adsorption capacity of 11.47 mg/g was achieved. The highest removal rate was 80.31% at initial phosphate concentration of 0.5 mg/L and adsorption of phosphate by orange peel biochars reached a maximum value of 8.61 mg/g at initial phosphate concentration of 1.0 mg/L. The elevation of pyrolysis temperature in peanut shell biochars enhances phosphate adsorption, while it exerted minimal influence on the adsorption efficiency of orange peel biochars. The findings suggest that the adsorption capacity of phosphate in biochars derived from peanut shells and orange peels is influenced by the concentration of adsorbed phosphate. These results are consistent with the studies conducted by Kizito et al. [37] and Mor et al. [38].

3.4. Adsorption kinetic model

The adsorption kinetic parameters are presented in Table 1, while the fitting curves of phosphate adsorption by peanut shell and orange peel biochars are illustrated in Fig. 4. The adsorption of phosphate by peanut shell and orange peel biochars followed the secondary kinetic model with a high R^2 value of 0.999, indicating chemical adsorption. The findings were consistent with the study conducted by Yi and Chen [39] on the use of agro-waste rice husk ash for phosphate removal from wastewater. The transfer of common electron pairs between the biochar-based adsorbent and the phosphate led to pollutant removal due to the formation of new chemical bonds [40].

Table 1
Parameters of adsorption kinetic model for phosphate adsorption by biochars

Biochar	First-order dynamic equation			Second-order dynamic equation		
	K_1 (min)	Q_e (mg/g)	R^2	K_2 (g/mg·min)	Q_e (mg/g)	R^2
Peanut shells	0.0940	5.98	0.975	0.0015	5.94	0.998
Orange peels	0.0891	5.68	0.970	0.0023	5.79	0.997

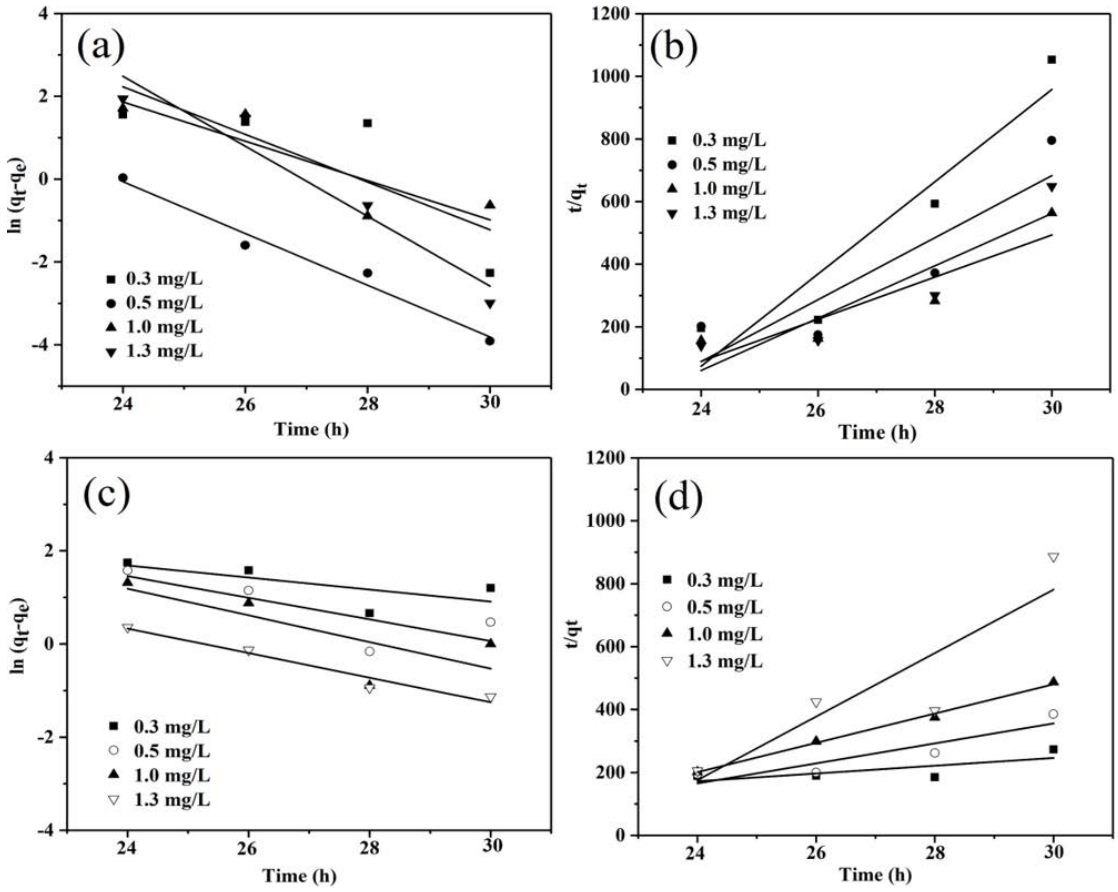

Fig. 4. Kinetic models of phosphate adsorption by biochars produced from peanut shells and orange peels.

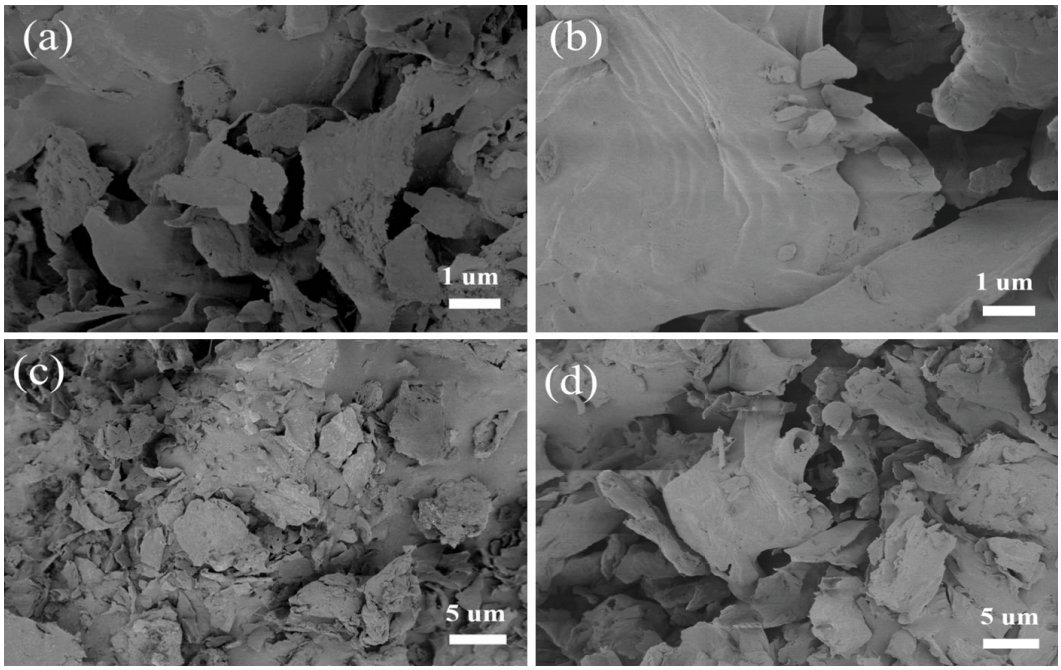

Fig. 5. Scanning electron microscopy images of biochars produced from peanut shells (a,c) and orange peels (b,d) at 400°C in 6 h.

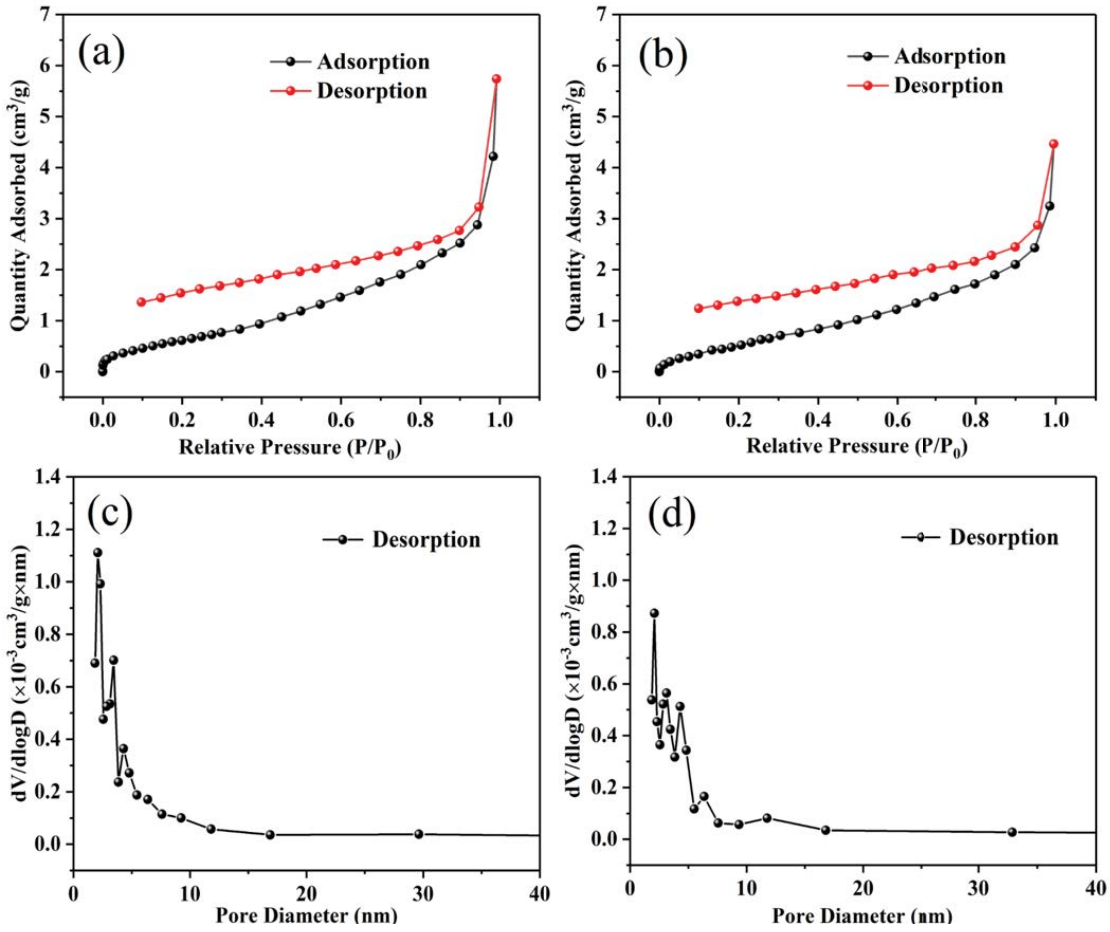

Fig. 6. Adsorption–desorption curves and pore sizes of biochars produced from peanut shells (a,c) and orange peels (b,d).

Table 2
Surface area, pore volume and pore size of the biochars produced from peanut shells and orange peels.

Sample	Surface area (m^2/g)	Pore volume (cm^3/g)	Pore size (nm)
Peanut shells	2.4968	0.0074	7.9238
Orange peels	2.4033	0.0054	7.1630

3.5. SEM analysis

Fig. 5 depicts the scanning electron microscope images of orange peel biochars heated at 300°C and peanut shell biochars heated at 400°C for a duration of 6 h. It is evident that the surface of the biochar exhibits a lamellar structure. As the magnification increases, the pore structure becomes increasingly dense and complex. This is due to the carbonization of biomass at a certain temperature, resulting in solid carbon and tar formation accompanied by gas volatilization that contributes to the development of pore structure. This improves the specific surface area to enhance the adsorption capacity significantly [41]. Upon comparison, it was observed that the granular pores of peanut shell biochars were more prominent, providing a larger surface area for the adsorption of phosphate. This finding is consistent with the superior adsorption performance of peanut shell biochars compared to orange peel biochars [42].

3.6. BET analysis

In order to examine the porous structure of the samples, N_2 adsorption and desorption tests were conducted for each sample and the resulting data has been summarized in Table 2 and Fig. 6. The BET measurement indicated that the specific surface areas of the biochars derived from peanut shells and orange peels were equivalent. The pore volume and size of the peanut shell biochars, however, exhibited a significantly greater magnitude compared to those of its orange peel counterparts, which was in accordance with the findings from SEM analysis. It is widely acknowledged that a pore size greater than 50 nm indicates a macroporous structure, while a pore size less than 50 nm demonstrates a mesoporous structure. Therefore, the peanut shell biochars exhibited macroporous characteristics, whereas the orange peel biochars possessed mesoporous properties. According to research, the macropores of peanut shell biochars were well-suited for efficient adsorption of phosphate due to their matching particle size.

4. Conclusions

The peanut shell biochars carbonized at 400°C for 6 h and orange peel biochars carbonized at 300°C for 6 h exhibited the highest yields of 86.7% and 81.2%, respectively. The peanut shell biochars produced at 400°C exhibited the highest phosphate removal performance, with a removal rate of 83.2% and an adsorption capacity of 5.94 mg/g under the conditions of an initial phosphate concentration of 0.5 mg/L, a biochar dosage of 5.0 g, and a contact time of 26 h. Conversely, under the same conditions of initial phosphate concentration, contact time, and biochar dosage, the orange peel biochars produced at 300°C demonstrated superior phosphate removal performance with a removal rate of 81.1% and an adsorption capacity of 5.79 mg/g. Contact time and initial phosphate concentration affected the process of phosphate adsorption. The whole adsorption processes of phosphate by peanut shell and orange peel biochars were well fitted with the second-order kinetic models, which were mainly chemical adsorption.

Acknowledgments

We gratefully thank financial supported by Applied Basic Research Plan of Liaoning (2023JH2/101300053), Science and Technology Plan of Shenyang (21-108-9-36), Major Original Program in Shenyang Normal University (ZD201904), the Ninth Batch of Education and Teaching Reform Project of Shenyang Normal University (JG2021-YB099), NSFC (22268003, 52272287, 22202138), Project from Yunnan Province (202301AT070027, 202305AF150116) and Dali University (KY2296129740).

References

[1] K. Qi, S.-y. Liu, R. Selvaraj, W. Wang, Z. Yan, Comparison of P_t and Ag as co-catalyst on g-C_3N_4 for improving photocatalytic activity: experimental and DFT studies, Desal. Water Treat., 153 (2019) 244–252.
[2] K. Qi, S.-y. Liu, R. Wang, Z. Chen, R. Selvaraj, P_t/g-C_3N_4 composites for photocatalytic H_2 production and $^{\bullet}OH$ formation, Desal. Water Treat., 154 (2019) 312–319.
[3] F.S. Ali, K. Qi, B. Al Wahaibi, M.A. Meetani, H. Al Lawati, Y. Kim, S.M.Z. Al Kindy, R. Selvaraj, Photocatalytic degradation of bisphenol A in the presence of TiO_2 nanoparticle: effect of solvent on size control, Desal. Water Treat., 79 (2017) 301–307.
[4] K. Qi, S. Karthikeyan, W. Kim, F.A. Marzouqi, I.S. Al-Khusaibi, Y. Kim, R. Selvaraj, Hydrothermal synthesis of SnS_2 nanocrystals for photocatalytic degradation of 2,4,6-trichlorophenol under white LED light irradiation, Desal. Water Treat., 92 (2017) 108–115.
[5] K. Qi, B. Sun, S.Y. Liu, M. Zhang, Research progress on carbon materials in tumor photothermal therapy, Biomed. Pharmacother., 165 (2023) 115070, doi: 10.1016/j.biopha.2023.115070.
[6] F. Yang, B. Yang, X. Gu, M. Li, K. Qi, Y. Yan, Detection of enrofloxacin residues in dairy products based on their fluorescence quenching effect on $AgInS_2$ QDs, Spectrochim. Acta, Part A, 301 (2023) 122985, doi: 10.1016/j.saa.2023.122985.
[7] N. Cui, A. Zada, J. Song, Y. Yang, M. Liu, Y. Wang, Y. Wu, K. Qi, R. Selvaraj, S.-y. Liu, G. Jin, Plasmon-induced ZnO-Ag/AgCl photocatalyst for degradation of tetracycline hydrochloride, Desal. Water Treat., 245 (2022) 247–257.
[8] R. Kayisier, Y. Ma, K. Qi, L. Xiao, Y. Wang, Y. Li, J. Li, Y. Li, Synergetic removal of mixed pollutants over cerium oxide/red phosphorus heterojunction composite, Vacuum, 213 (2023) 112086, doi: 10.1016/j.vacuum.2023.112068.
[9] Y. Ma, X. Aihemaiti, K. Qi, S. Wang, Y. Shi, Z. Wang, M. Gao, F. Gai, Y. Qiu, Construction of oxygen-vacancies-rich S-scheme $BaTiO_3$/red phosphorous heterojunction for enhanced photocatalytic activity, J. Mater. Sci. Technol., 156 (2023) 217–229.
[10] K. Qi, C. Zhuang, M. Zhang, P. Gholami, A. Khataee, Sonochemical synthesis of photocatalysts and their applications, J. Mater. Sci. Technol., 123 (2022) 243–256.
[11] J. Zhang, A. Bifulco, P. Amato, C. Imparato, K. Qi, Copper indium sulfide quantum dots in photocatalysis, J. Colloid Interface Sci., 638 (2023) 193–219.

[12] W. Xiang, X. Zhang, J. Chen, W. Zou, F. He, X. Hu, D.C.W. Tsang, Y.S. Ok, B. Gao, Biochar technology in wastewater treatment: a critical review, Chemosphere, 252 (2020) 126539, doi: 10.1016/j.chemosphere.2020.126539.
[13] J. Zhang, X. Gu, Y. Zhao, K. Zhang, Y. Yan, K. Qi, Photocatalytic hydrogen production and tetracycline degradation using $ZnIn_2S_4$ quantum dots modified g-C_3N_4 composites, Nanomaterials, 13 (2023) 305, doi: 10.3390/nano13020305.
[14] D. Mohan, A. Sarswat, Y.S. Ok, C.U. Pittman Jr., Organic and inorganic contaminants removal from water with biochar, a renewable, low cost and sustainable adsorbent-a critical review, Bioresour. Technol., 160 (2014) 191–202.
[15] I. Khalaf Erabee, Removal of ammonia nitrogen NH-N and hexavalent chromium(VI) from wastewater using agricultural waste activated carbon, Orient. J. Chem., 34 (2018) 1033–1040.
[16] C. Arora, P. Kumar, S. Soni, J. Mittal, A. Mittal, B. Singh, Efficient removal of malachite green dye from aqueous solution using *Curcuma caesia* based activated carbon, Desal. Water Treat., 195 (2020) 341–352.
[17] H. Daraei, A. Mittal, Investigation of adsorption performance of activated carbon prepared from waste tire for the removal of methylene blue dye from wastewater, Desal. Water Treat., 90 (2017) 294–298.
[18] A. Patel, S. Soni, J. Mittal, A. Mittal, C. Arora, Sequestration of crystal violet from aqueous solution using ash of black turmeric rhizome, Desal. Water Treat., 220 (2021) 342–352.
[19] Saifullah, S. Dahlawi, A. Naeem, Z. Rengel, R. Naidu, Biochar application for the remediation of salt-affected soils: challenges and opportunities, Sci. Total Environ., 625 (2018) 320–335.
[20] M. Ullah, R. Nazir, M. Khan, W. Khan, M. Shah, S.G. Afridi, A. Zada, The effective removal of heavy metals from water by activated carbon adsorbents of *Albizia lebbeck* and *Melia azedarach* seed shells, Soil Water Res., 15 (2020) 30–37.
[21] R. Ahmad, I. Hasan, A. Mittal, Adsorption of Cr(VI) and Cd(II) on chitosan grafted polyaniline-OMMT nanocomposite: isotherms, kinetics and thermodynamics studies, Desal. Water Treat., 58 (2017) 144–153.
[22] A. Dang, X. liu, Y. Wang, Y. Liu, T. Cheng, A. Zada, F. Ye, W. Deng, Y. Sun, T. Zhao, T. Li, High-efficient adsorption for versatile adsorbates by elastic reduced graphene oxide/Fe_3O_4 magnetic aerogels mediated by carbon nanotubes, J. Hazard. Mater., 457 (2023) 131846, doi: 10.1016/j.jhazmat.2023.131846.
[23] X. He, J. Xia, J. He, K. Qi, A. Peng, Y. Liu, Highly efficient capture of heavy metal ions on amine-functionalized porous polymer gels, Gels, 9 (2023) 297, doi: 10.3390/gels9040297.
[24] J. Mittal, R. Ahmad, A. Mariyam, V.K. Gupta, A. Mittal, Expeditious and enhanced sequestration of heavy metal ions from aqueous environment by papaya peel carbon: a green and low cost adsorbent, Desal. Water Treat., 210 (2021) 365–376.
[25] J. Mittal, R. Ahmad, A. Mittal, Kahwa tea (*Camellia sinensis*) carbon — a novel and green low-cost adsorbent for the sequestration of titan yellow dye from its aqueous solutions, Desal. Water Treat., 227 (2021) 404–411.
[26] R. Nazir, M. Khan, R. Ur Rehman, S. Shujah, M. Khan, M. Ullah, A. Zada, N. Mahmood, I. Ahmad, Adsorption of selected azo dyes from an aqueous solution by activated carbon derived from *Monotheca buxifolia* waste seeds, Soil Water Res., 15 (2020) 166–172.
[27] Y.P. Gong, Z.Y. Ni, Z.Z. Xiong, L.H. Cheng, X.H. Xu, Phosphate and ammonium adsorption of the modified biochar based on *Phragmites australis* after phytoremediation, Environ. Sci. Pollut. Res. Int., 24 (2017) 8326–8335.
[28] R. He, Z. Peng, H. Lyu, H. Huang, Q. Nan, J. Tang, Synthesis and characterization of an iron-impregnated biochar for aqueous arsenic removal, Sci. Total Environ., 612 (2018) 1177–1186.
[29] T. Sizmur, T. Fresno, G. Akgul, H. Frost, E. Moreno-Jimenez, Biochar modification to enhance sorption of inorganics from water, Bioresour. Technol., 246 (2017) 34–47.
[30] Y. Liu, W. Gao, R. Liu, W. Zhang, J. Niu, X. Lou, G. Li, H. Liu, Z. Li, Removal of phosphorus using biochar derived from Fenton sludge: mechanism and performance insights, Water Environ. Res., 94 (2022) 10763, doi: 10.1002/wer.10763.
[31] N. Zhu, T. Yan, J. Qiao, H. Cao, Adsorption of arsenic, phosphorus and chromium by bismuth impregnated biochar: adsorption mechanism and depleted adsorbent utilization, Chemosphere, 164 (2016) 32–40.
[32] S. Wang, L. Kong, J. Long, M. Su, Z. Diao, X. Chang, D. Chen, G. Song, K. Shih, Adsorption of phosphorus by calcium-flour biochar: isotherm, kinetic and transformation studies, Chemosphere, 195 (2018) 666–672.
[33] L. Dai, F. Tan, H. Li, N. Zhu, M. He, Q. Zhu, G. Hu, L. Wang, J. Zhao, Calcium-rich biochar from the pyrolysis of crab shell for phosphorus removal, J. Environ. Manage., 198 (2017) 70–74.
[34] J.O. Eduah, E.K. Nartey, M.K. Abekoe, H. Breuning-Madsen, M.N. Andersen, Phosphorus retention and availability in three contrasting soils amended with rice husk and corn cob biochar at varying pyrolysis temperatures, Geoderma, 341 (2019) 10–17.
[35] A.U. Rajapaksha, S.S. Chen, D.C. Tsang, M. Zhang, M. Vithanage, S. Mandal, B. Gao, N.S. Bolan, Y.S. Ok, Engineered/designer biochar for contaminant removal/immobilization from soil and water: potential and implication of biochar modification, Chemosphere, 148 (2016) 276–291.
[36] M. Zhang, B. Gao, Removal of arsenic, methylene blue, and phosphate by biochar/AlOOH nanocomposite, Chem. Eng. J., 226 (2013) 286–292.
[37] S. Kizito, S. Wu, W. Kipkemoi Kirui, M. Lei, Q. Lu, H. Bah, R. Dong, Evaluation of slow pyrolyzed wood and rice husks biochar for adsorption of ammonium nitrogen from piggery manure anaerobic digestate slurry, Sci. Total Environ., 505 (2015) 102–112.
[38] S. Mor, K. Chhoden, K. Ravindra, Application of agro-waste rice husk ash for the removal of phosphate from the wastewater, J. Cleaner Prod., 129 (2016) 673–680.
[39] M. Yi, Y. Chen, Enhanced phosphate adsorption on Ca-Mg-loaded biochar derived from tobacco stems, Water Sci. Technol., 78 (2018) 2427–2436.
[40] Z. Li, X. Liu, Y. Wang, Modification of sludge-based biochar and its application to phosphorus adsorption from aqueous solution, J. Mater. Cycles Waste Manage., 22 (2019) 123–132.
[41] M.T. Yagub, T.K. Sen, M. Ang, Removal of cationic dye methylene blue (MB) from aqueous solution by ground raw and base modified pine cone powder, Environ. Earth Sci., 71 (2013) 1507–1519.
[42] P. Zhang, D. O'Connor, Y. Wang, L. Jiang, T. Xia, L. Wang, D.C.W. Tsang, Y.S. Ok, D. Hou, A green biochar/iron oxide composite for methylene blue removal, J. Hazard. Mater., 384 (2020) 121286, doi: 10.1016/j.jhazmat.2019.121286.